


Comparison of Intravoxel Incoherent Motion Imaging and Multiecho Dynamic Contrast-Based MRI in Rectal Cancer

Kine Mari Bakke, MSc,^{1,2*}  Endre Grøvik, PhD,^{3,4} Sebastian Meltzer, MD, PhD,¹ Anne Negård, MD, PhD,^{5,6} Stein Harald Holmedal, MD,⁵ Lars Tore G. Mikalsen, PhD,³ Lars Gustav Lyckander, MD,⁷ Anne H. Ree, MD, PhD,^{1,6} Kjell-Inge Gjesdal, PhD,^{1,8} Kathrine R. Redalen, PhD,^{1,9} and Atle Bjørnerud, PhD^{2,3}

Background: Dynamic contrast-based MRI and intravoxel incoherent motion imaging (IVIM) MRI are both methods showing promise as diagnostic and prognostic tools in rectal cancer. Both methods aim at measuring perfusion-related parameters, but the relationship between them is unclear.

Purpose: To investigate the relationship between perfusion- and permeability-related parameters obtained by IVIM-MRI, T₁-weighted dynamic contrast-enhanced (DCE)-MRI and T₂*-weighted dynamic susceptibility contrast (DSC)-MRI.

Study Type: Prospective.

Subjects: In all, 94 patients with histologically confirmed rectal cancer.

Field Strength/Sequence: Subjects underwent pretreatment 1.5T clinical procedure MRI, and in addition a study-specific diffusion-weighted sequence ($b = 0, 25, 50, 100, 500, 1000, 1300 \text{ s/mm}^2$) and a multiecho dynamic contrast-based echo-planar imaging sequence.

Assessment: Median tumor values were obtained from IVIM (perfusion fraction [f], pseudodiffusion [D^*], diffusion [D]), from the extended Tofts model applied to DCE data (K^{trans} , k_{ep} , v_p , v_e) and from model free deconvolution of DSC (blood flow [BF] and area under curve). A subgroup of the excised tumors underwent immunohistochemistry with quantification of microvessel density and vessel size.

Statistical Test: Spearman's rank correlation test.

Results: D^* was correlated with BF ($r_s = 0.47$, $P < 0.001$), and f was negatively correlated with k_{ep} ($r_s = -0.31$, $P = 0.002$). BF was correlated with K^{trans} ($r_s = 0.29$, $P = 0.004$), but this correlation varied extensively when separating tumors into groups of low ($r_s = 0.62$, $P < 0.001$) and high ($r_s = -0.06$, $P = 0.68$) BF . K^{trans} was negatively correlated with vessel size ($r_s = -0.82$, $P = 0.004$) in the subgroup of tumors with high BF .

Data Conclusion: We found an association between D^* from IVIM and BF estimated from DSC-MRI. The relationship between IVIM and DCE-MRI was less clear. Comparing parameters from DSC-MRI and DCE-MRI highlights the importance of the underlying biology for the interpretation of these parameters.

Level of Evidence: 2

Technical Efficacy Stage: 1

J. MAGN. RESON. IMAGING 2019;50:1114–1124.

THE USE OF dynamic contrast-enhanced magnetic resonance imaging (DCE-MRI) has shown potential for obtaining predictive and prognostic biomarkers in rectal cancer. This method has enabled estimation of parameters

with the ability to predict histopathologic treatment outcome to preoperative chemoradiotherapy¹ and distinguish between tumor differentiation grades.² These results indicate that DCE-MRI may be a tool to enable further

View this article online at wileyonlinelibrary.com. DOI: 10.1002/jmri.26740

Received Oct 18, 2018, Accepted for publication Mar 21, 2019.

*Address reprint requests to: K.M.B., Sykehusveien 25, 1478, Lørenskog; Norway. E-mail: kinemb@fys.uio.no

From the ¹Department of Oncology, Akershus University Hospital, Lørenskog, Norway; ²Department of Physics, University of Oslo, Oslo, Norway; ³Department of Diagnostic Physics, Division of Radiology and Nuclear Medicine, Oslo University Hospital, Oslo, Norway; ⁴Department of Optometry, Radiography and Lighting Design, University of South-Eastern Norway, Drammen, Norway; ⁵Department of Radiology, Akershus University Hospital, Lørenskog, Norway; ⁶Institute of Clinical Medicine, University of Oslo, Oslo, Norway; ⁷Department of Pathology, Akershus University Hospital, Lørenskog, Norway; ⁸Sunnmøre MR-klinikk, Ålesund, Norway; and ⁹Department of Physics, Norwegian University of Science and Technology, Trondheim, Norway

This is an open access article under the terms of the Creative Commons Attribution-NonCommercial License, which permits use, distribution and reproduction in any medium, provided the original work is properly cited and is not used for commercial purposes.

treatment individualization in rectal cancer at the time of diagnosis.

DCE-MRI aims at estimating capillary permeability by measuring the rate of extravasation of an intravenously injected gadolinium-based contrast agent (GBCA). However, for patients with impaired kidney function there are contraindications to these types of contrast agents, and in addition there are some concerns regarding the safety and long-term retention of GBCA.^{3,4} This encourages investigation of alternative noncontrast agent-based approaches for obtaining functional MRI-derived biomarkers.

In recent years the concept of intravoxel incoherent motion (IVIM) imaging has received growing attention. IVIM is an expansion of conventional diffusion-weighted imaging (DWI) whereby intravascular water reflecting microcirculatory properties can be separated from extravascular water due to different diffusion properties.⁵ IVIM-based DWI has shown promise as a completely noninvasive approach for obtaining perfusion-related information⁶ and is thus clearly an attractive technique both in terms of reduced cost as well as patient safety compared with methods requiring contrast agent injections.

The relationship between IVIM-derived perfusion metrics and the more conventional contrast agent (CA)-based methods for measuring perfusion-related parameters with MRI remains unclear. According to a recent review by Federau,⁷ the strongest correlation between IVIM- and CA-based perfusion metrics in human studies has been reported in brain tumors using the dynamic susceptibility contrast (DSC)-MRI method. DSC-MRI is a CA-based method whereby the T_2^* - (susceptibility) effect, rather than the T_1 -effect of the CA, is utilized to measure perfusion-related metrics. DSC-MRI has mainly been used in the brain due to dominant T_2^* -effects in regions with an intact blood-brain barrier,⁸ but has recently also shown utility in staging of rectal cancer.⁹ Specifically addressing brain tumors, Bisdas et al¹⁰ found good correlation between perfusion measured by DSC-MRI and IVIM-derived metrics but generally poorer correlation between DCE-MRI-derived metrics and IVIM. Also, for applications outside the central nervous system (CNS), the correlations between IVIM and DCE-MRI-derived metrics are generally unclear.^{11,12} Although some DCE-MRI models can be used to estimate perfusion and tissue blood volume, most DCE-MRI studies focus on measurement of permeability-related metrics and their correlation with IVIM-related parameters may be less obvious. Further, DCE-MRI is generally hampered by poor reproducibility and lack of standardization with respect to the choice of kinetic model and acquisition protocol.¹³

The purpose of the present work was to examine the associations between perfusion-related parameters measured by IVIM with those obtained from DSC- and DCE-MRI in patients with rectal cancer. By using a multiecho dynamic contrast-based sequence, both DSC- and DCE-derived metrics

were obtained in a single acquisition, thereby potentially providing more accurate comparisons between the different methods.

Materials and Methods

Patients

This investigation was part of a prospective biomarker study enrolling 192 patients with suspected rectal cancer between October 2013 and December 2017. Excluding cases without histologically confirmed rectal cancer ($n = 19$) or with study withdrawal ($n = 4$), nonconsistent MRI sequence due to set-up of experiment ($n = 23$), poor quality of dynamic images ($n = 20$), difficulties in coregistration due to bowel movement or tumor volume $< 5 \text{ cm}^3$ ($n = 6$), and other incidental difficulties encountered during the clinical MRI acquisition (eg, patients medically ineligible for or refusing contrast administration, software updates disarranging the timing of contrast administration) ($n = 26$), a total of 94 patients were included in this report. The MRI was acquired at baseline before any treatment had been initiated.

The study was performed in accordance with the Helsinki Declaration and written informed consent was obtained from all patients. Approval was obtained from the Institutional Review Board and the Regional Committee for Medical and Health Research Ethics.

MRI

MRI was performed with a Philips Achieva 1.5T system (Philips Healthcare, Best, The Netherlands). To reduce bowel movement, patients were given glucagon (1 mg/ml, 1 mL intramuscularly) and Buscopan (10 mg/ml, 1 mL intravenously) before scanning, and an equivalent dose of Buscopan before commencement of the dynamic acquisition.

The patients underwent MRI according to clinical procedure, including a high-resolution T_2 -weighted sequence perpendicular to the tumor axis used for tumor delineation. In addition, the patients underwent a multiecho dynamic contrast-based MRI with GBCA injection and an extended DWI sequence.

DWI was obtained with seven b-values, $b = 0, 25, 50, 100, 500, 1000, 1300 \text{ s/mm}^2$, echo time (TE) = 75 msec, repetition time (TR) = 3 sec, and 6 averages. The acquired matrix size was 80×60 over a $160 \times 160 \text{ mm}^2$ field of view and a 4 mm slice thickness, giving a spatial resolution of $2.00 \times 2.67 \times 4.00 \text{ mm}^3$.

The dynamic sequence was obtained as a 3D multishot echo planar imaging sequence with three echoes, TE = 4.6, 13.9, 23.2 msec, TR = 39 msec, flip angle 39° , time resolution that varied between 1.9 and 2.5 sec, with -60 repetitions. The acquired matrix size was 92×90 over a $180 \times 180 \text{ mm}^2$ field of view and a 10 mm slice thickness, giving a spatial resolution of $1.96 \times 2.00 \times 10 \text{ mm}^3$. A dose of 0.2 mL/kg body weight of GBCA (Dotarem, 279.3 mg/mL, Guerbet Roissy, France) was injected as a bolus directly followed by a 20-mL saline solution.

Image Postprocessing

The acquired multiecho data was used to extract two dynamic time series by least-square fitting from the equation:

$$S(t, TE_n) = M_0(t) e^{-TE_n/T_2^*(t)} \quad (1)$$

where $S(t, TE_n)$ is the acquired signal, n is the echo number, and $M_0(t)$ is the T_1 -weighted signal corrected for effects from T_2^* -

relaxation. In addition to T_1 -weighted DCE analysis, this fit also allowed estimation of the dynamic $R_2^*(t) = 1/T_2^*(t)$ signal used for DSC analysis.

DSC-MRI. Assuming a linear relationship between the change in $R_2^*(t)$ and CA concentration to obtain semiquantitative parameters, the blood flow (BF) was calculated using the established tracer kinetic model for DSC-MRI¹⁴:

$$C_t(t) = \beta f \int_0^t AIF(\tau) R(t-\tau) d\tau \quad (2)$$

where $C_t(t)$ is the CA concentration in tissue, $AIF(t)$ is the arterial input function (CA concentration in a feeding artery), $R(t)$ is the residue function, and β is an unknown scaling factor. f is the fractional flow value and is related to tissue blood flow (perfusion, BF) according to:

$$BF = f \frac{k_h}{\rho} \quad (3)$$

where ρ is the tissue density (g/ml) and k_h is the hematocrit scaling factor between large and small blood vessels,¹⁵ and was assumed to be constant. Since the values of β and k_h are not known, the resulting BF values should be regarded as relative perfusion estimates.

The AIF was obtained individually from a nearby artery using an automatic cluster-algorithm.¹⁶ The convolution integral was solved using circular singular value decomposition.¹⁷ Area under curve (AUC) for 30 and 60 seconds was calculated as an approximation of tissue blood volume as:

$$AUC = \frac{\int_0^t C_t(\tau) d\tau}{\int_0^t AIF(\tau) d\tau} \quad (4)$$

where the lower integration limit was set at bolus arrival time and the upper integration limit was set at 30 and 60 seconds, respectively.

DCE-MRI. The $M_0(t)$ signal was then used to estimate the CA concentration using the signal equation for a spoiled gradient echo (SPGR) sequence without T_2^* relaxation contribution:

$$S_{SPGR}(t) = M_0(t) \frac{\sin \alpha \left(1 - e^{-\frac{TR}{T_1(t)}}\right)}{1 - e^{-\frac{TR}{T_1(t)}} \cos \alpha} \quad (5)$$

As for the DSC analysis, a linear relationship was assumed between the change in $R_1 = 1/T_1$ and CA concentration, and an average precontrast T_1 -value measured from six patients was used (1350 msec in tissue).⁹

The extended Tofts (ET) model¹⁸ was fitted to the data with the equation:

$$C_t(t) = v_p AIF(t) + K^{trans} \int_0^t e^{-\tau k_{ep}} AIF(\tau) d\tau \quad (6)$$

where K^{trans} is the transfer constant between blood plasma and the interstitial space, k_{ep} the rate constant, and v_p the blood plasma volume. These parameters relate to the extracellular, extravascular space, v_e , as $v_e = K^{trans}/k_{ep}$. The same individual AIF as for the DSC analysis was used.

The DCE and DSC-MRI analyses were done in nordicICE (NordicNeuroLab, Bergen, Norway).

IVIM. The DWI signal was fitted to the equation:

$$\frac{S(b)}{S_0} = f e^{-bD^*} + (1-f) e^{-bD} \quad (7)$$

where f is the perfusion fraction, D^* is the pseudodiffusion coefficient, and D is the diffusion coefficient. We also calculated the product of the perfusion fraction and pseudodiffusion, $f \times D^*$. The fit was done in MatLab (R2015a, MathWorks, Natick, MA) using a Levenberg–Marquardt algorithm. To check for consistency of the results, the exponential fit was performed both with and without $b = 1300 \text{ s/mm}^2$.

Tumor delineation was done by two radiologists with 14 and 7 years of experience on T_2 -weighted images, with the DWI serving as extra guidance. The resultant tumor regions were then semiautomatically coregistered to the other image sequences for optimal fit, also done in nordicICE.

Immunohistochemistry

After surgery, 17 tumors were randomly selected for immunohistochemistry (IHC). Formalin-fixed paraffin-embedded tissue sections (4 μm thick) were deparaffinized and hydrated followed by heat-induced epitope retrieval (20 min at 97°C, 3-in-1 procedure) in Dako (Carpinteria, CA) PT-link with target retrieval solution with high pH (code K8004). Incubation time with the primary antibody was 30 minutes and with the secondary antibody/HRP it was 20 minutes. Counterstaining was performed with Hagens hematoxylin (5 min, diluted 1:4). Staining with CD34 (mouse monoclonal antibody, clone QBEnd/10, Nordic BioSite, Sweden) was performed with the Autostainer Link 48 (Dako) using the Dako Envision Flex Code 8000 visualization kit. Appropriate controls were included and showed satisfactory results. The slides were scanned using the Aperio Scanscope AT using a 20x/0.75 objective with a 0.50 $\mu\text{m}/\text{pixel}$ resolution. Microvessel density (MVD) and average vessel size were extracted from the scanned slides by an automated and adapted MatLab script.¹⁹

Statistical Analysis

Consistency in tumor delineation and reproducibility of the individual parameters for the two radiologists was evaluated with intraclass correlation tests. Correlations between parameters were investigated using Spearman rank correlation test. Results were deemed statistically significant if $P < 0.01$, to lower risk of false positives due to multiple testing. All statistical procedures were done in SPSS (v. 25, IBM, Armonk, NY).

Results

Patient demographics are given in Table 1. Estimated kinetic parameters obtained from the tumor volumes defined by the

TABLE 1. Patient Demographics for the Study

Number of patients	94
Females	33 (35%)
Males	61 (65%)
Age (median)	65 years
Disease stage	
T2	14 (15%)
T3	46 (49%)
T4	34 (36%)
N0	39 (42%)
N1	33 (35%)
N2	22 (23%)
M0	71 (76%)
M1	23 (24%)

two radiologists were highly correlated (Table 2), and therefore only one set of parameter results is reported. The IVIM parameters showed only linear shifts towards higher D^* , and

lower f and D , when omitting $b = 1300 \text{ s/mm}^2$ compared with using all seven b -values. The correlation between the set of IVIM parameters (f, D, D^*) estimated from six and seven b -values was high (>0.90) and the associations with other parameters (from DCE- and DSC-MRI) showed the same trends. The results reported in the following are from all seven b -values.

Median values and interquartile ranges for all calculated parameters are given in Table 2 and examples of parameter images overlaid on T_2 -weighted images are shown in Fig. 1. Spearman's rank correlation coefficients (r_s) and P -values for comparisons between parameters are given in Tables 3–5, and scatterplots of the most significant findings are presented in Fig. 2. From IVIM, the pseudodiffusion coefficient D^* was correlated with BF from the DSC-analysis ($r_s = 0.47; P < 0.001$) (Table 3), and the perfusion fraction f showed a negative correlation with k_{ep} from the DCE-analysis ($r_s = -0.31; P < 0.002$) (Table 4). The comparison of parameters from DSC-MRI and DCE-MRI (Table 5) revealed a correlation between BF and K^{trans} ($r_s = 0.29; P = 0.004$), and between BF and v_p ($r_s = 0.44; P < 0.001$). Both AUC_{30} and AUC_{60} correlated with v_e ($r_s = 0.34; P = 0.001$, and $r_s = 0.45; P < 0.001$, respectively) and, in the case of AUC_{60} , also a negative correlation with k_{ep} ($r_s = -0.45; P < 0.001$). Theoretically, BF and K^{trans} are only associated in a flow limited regime²⁰ (low

TABLE 2. Estimated values

	Median values (25th - 75th percentile)	ICC (confidence interval)
IVIM		
f (fraction)	0.33 (0.30–0.37)	0.96 (0.95–0.98)
D^* ($10^{-3} \text{ mm}^2/\text{s}$)	12.11 (9.87–14.35)	0.97 (0.95–0.98)
$f \times D^*$ ($10^{-3} \text{ mm}^2/\text{s}$)	3.75 (2.93–4.57)	0.98 (0.97–0.99)
D ($10^{-3} \text{ mm}^2/\text{s}$)	0.60 (0.50–0.71)	0.98 (0.96–0.98)
DSC		
BF (ml/min/100g)	107.06 (78.32–135.80)	0.97 (0.95–0.98)
AUC_{30} (a. u.)	0.12 (0.03–0.22)	0.96 (0.93–0.97)
AUC_{60} (a. u.)	0.55 (0.31–0.80)	0.93 (0.90–0.96)
DCE		
K^{trans} (min^{-1})	0.04 (0.02–0.06)	0.96 (0.94–0.97)
k_{ep} (min^{-1})	0.24 (0.11–0.38)	0.96 (0.94–0.97)
v_p (%)	0.11 (0.05–0.17)	0.96 (0.94–0.98)
v_e (%)	10.58 (5.68–15.49)	0.59 (0.38–0.73)

Median values based on tumor delineations from one radiologist and intraclass correlation coefficients (ICC) between the two radiologists. f = perfusion fraction, D^* = pseudodiffusion coefficient, D = diffusion coefficient, BF = relative blood flow, AUC_{30}/AUC_{60} = area under curve for 30 and 60 seconds, respectively, after bolus arrival (a. u. = arbitrary units), K^{trans} = transfer constant between blood plasma and the interstitial space, k_{ep} = rate constant, v_p = blood plasma volume, v_e = extracellular, extravascular space.

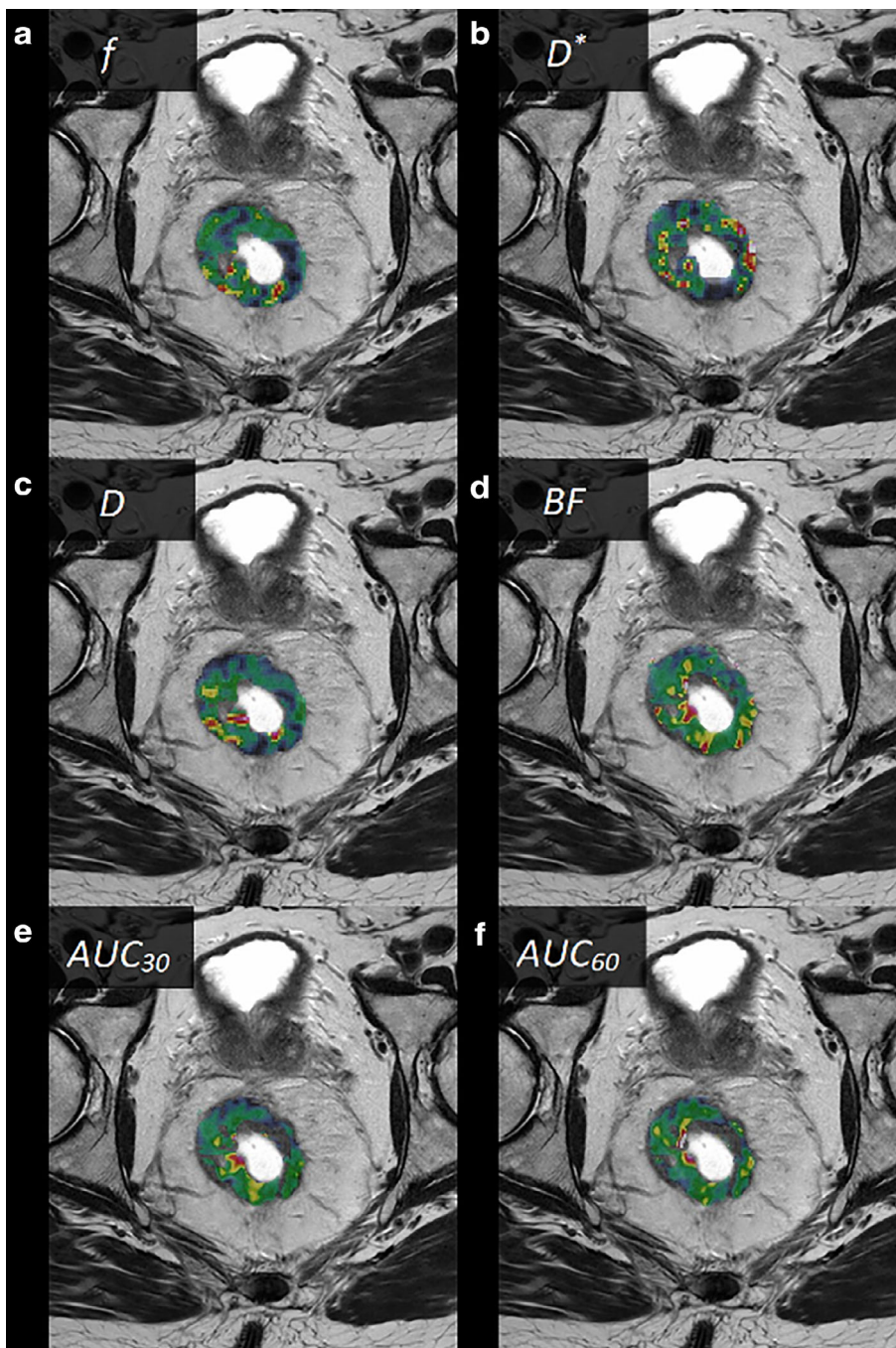


FIGURE 1: Examples of parametric images from a male patient with a T3 rectal tumor (parametric images of the tumor area shown as color overlays on T₂-weighted images), (a) f , (b) D^* , (c) D , (d) BF , (e) AUC_{30} , (f) AUC_{60} , (g) K^{trans} , (h) k_{ep} , (i) v_p , and (j) v_e .

perfusion). The correlation between BF and K^{trans} was stronger ($r_s = 0.62$, $P < 0.001$) when analyzing tumors with $BF < 100$ ml/min/100 g, corresponding to the lower half of the population ($n = 47$) (Fig. 3). When analyzing the other half of the population ($BF > 100$ ml/min/100 g), no correlation between these parameters was found ($r_s = -0.06$, $P = 0.68$).

Of the 17 tumor specimens analyzed by IHC, 12 had a full set of MRI parameters for correlation analysis. There was no correlation between MVD or vessel size and any MRI-derived parameters. However, when looking at tumors with $BF > 100$ ml/min/100 g ($n = 10$), we observed a negative

correlation between vessel size and K^{trans} ($r_s = -0.82$, $P = 0.004$) (Fig. 4).

Discussion

A main result from this study of 94 rectal tumors is the correlation between D^* from IVIM imaging and BF from DSC-MRI. This is in line with the findings of Bisdas et al,¹⁰ where a strong correlation between these parameters was found in glioblastomas. To our knowledge, this relationship has so far not been examined outside the CNS. The validity of

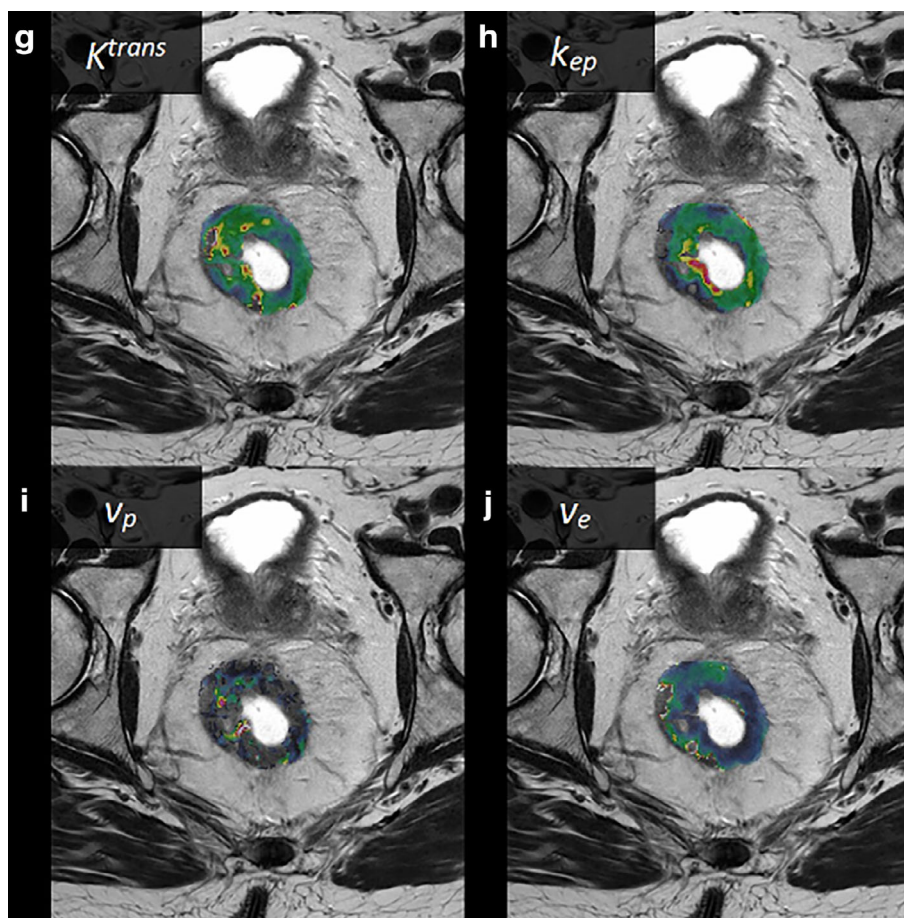


FIGURE 1: (Continued)

measuring perfusion with the IVIM-method has been questioned,²¹ and we show here that there at least exists a linear relationship between the pseudodiffusion coefficient and perfusion estimated by contrast-based MRI.

Previous studies have examined the link between IVIM imaging and DCE-MRI, with varying results,^{10,11,22} possibly reflecting the numerous qualitative and quantitative methods used to analyze DCE data. In addition, the interpretation of the parameters from DCE-MRI can vary depending on the underlying biology. In particular, K^{trans} will reflect tissue blood flow if tissue perfusion is low relative to the permeability surface area product (flow-limited regime), and conversely will

reflect permeability if tissue perfusion is high relative to the permeability surface area product (permeability-limited regime).²⁰ In the limiting condition of a pure permeability-limited regime, perfusion and permeability are therefore expected to be uncorrelated. The results from our data suggest that blood flow in this population of rectal tumors spans both these regimes, where low BF in tumors was strongly correlated with K^{trans} , and high tumor BF was not correlated, suggesting that the heterogeneity of rectal cancers makes it challenging to interpret results in studies focusing only on DCE-MRI. There was no significant correlation between MVD and K^{trans} , in line with a report by Kim et al,²³ but we observed a strong negative correlation between K^{trans} and vessel size in tumors with high perfusion. The cases for this analysis were in the high BF group where K^{trans} is only expected to be dependent on permeability and surface area of the vessels.¹⁸ The higher leakage from smaller vessels may be explained by their larger ratio of circumference to cross-section measures compared with larger vessels, and hence larger surface area per unit blood volume. No other MRI-derived parameters were correlated with MVD or vessel size, which may reflect that MRI parameters in general are measured in in vivo functional tissue, and therefore will not be adequately represented in ex vivo resected tissue.

TABLE 3. Correlations between IVIM- and DSC-MRI

	BF	AUC_{30}	AUC_{60}
f	-0.03 (0.80)	-0.03 (0.79)	0.12 (0.26)
D^*	0.47 (<0.001)	0.15 (0.15)	0.22 (0.03)
$f \times D^*$	0.38 (<0.001)	0.09 (0.41)	0.23 (0.03)
D	-0.23 (0.03)	0.05 (0.61)	-0.07 (0.52)

Spearman's Rank Correlation Coefficients r_s (P-values in parenthesis)

TABLE 4. Correlations between IVIM- and DCE-MRI

	K^{trans}	k_{ep}	v_p	v_e
f	-0.22 (0.03)	-0.31 (0.002)	-0.17 (0.10)	0.23 (0.03)
D^*	-0.18 (0.09)	0.06 (0.54)	0.12 (0.27)	-0.16 (0.13)
$f \times D^*$	-0.28 (0.007)	-0.10 (0.32)	0.01 (0.97)	-0.01 (0.98)
D	0.03 (0.81)	-0.11 (0.28)	-0.12 (0.25)	0.13 (0.19)

Spearman's Rank Correlation Coefficients r_s (P-values in parenthesis)

We further observed a correlation between BF and v_p . This is not surprising, since an increase in plasma volume would lead to a similar increase in tissue perfusion for constant blood supply. It should be noted that the ET model used to estimate v_p and permeability is only strictly valid in the limiting case of very high tissue blood flow (negligible mean capillary transit time, MTT).²⁰ Since blood flow estimates are independent of MTT, any correlations between BF and DCE-parameters derived using the ET model may be biased by local variations in tissue MTT. In particular, the measured parameter v_p may therefore reflect a mixture of blood volume and plasma flow. Using a more complex kinetic model, like the two-compartment exchange model, might account for MTT variations and also provide direct estimates of tissue perfusion from the DCE data,²⁰ but we question whether our data supports the use of an even more complex model.

In some reports about the relationship between IVIM- and DCE-MRI parameters,^{24,25} the focus has been on the correlation between the perfusion fraction f from IVIM and blood volume from DCE, as this is the expected theoretical relationship according to one of the original works of Le Bihan and Turner.²⁶ The hypothesis that v_p derived from the ET model likely reflects a combination of both blood flow and blood volume could be a possible reason for the absence of this correlation between f and v_p in our data. In the model-free deconvolution approach in DSC-MRI the blood volume is normally estimated by the integration over the contrast curve, normalized by the area of the AIF. This approach assumes that the contrast agent is confined to the intravascular space for the duration of the measurement, and thus the DSC approach has to date been mostly used in CNS

applications where the intact blood-brain barrier prevents CA leakage. We used a similar approach to estimate tissue AUC, integrated over both 30 and 60 seconds, normalized to the area of the AIF. However, due to CA extravasation, this AUC does not reflect tissue blood volume alone but rather the combined volume of the intravascular and extravascular, extracellular volume fractions. This is reflected in our results by the correlation between both AUC_{30} and AUC_{60} and the extracellular, extravascular volume fraction v_e and the negative correlation with the CA reflux constant k_{ep} . We did not correct for CA leakage in the DSC-based perfusion analysis, since BF obtained from AIF deconvolution, to a first approximation, can be assumed to be independent of CA leakage.²⁷ Further, current kinetic model-based leakage correction methods applied to blood volume estimates from normalized tissue response time integrals rely on identification of a reference area with no CA leakage effects.²⁸ These methods are thus not readily applicable to non-CNS applications since nonleaky reference regions cannot be obtained.

From this, it is concluded that estimation of pure intravascular blood volume is challenging using both DCE- and DSC-MRI outside the CNS, limiting the ability to show the expected correlation with IVIM-derived perfusion fraction f .²⁶ We did, however, find a weak negative correlation between f and the rate constant k_{ep} , and between $f \times D^*$ and K^{trans} , without being able to find a biological reasoning behind this result. Recently, Sun et al²² investigated the relationship between IVIM and DCE-MRI in a comparable cohort of rectal cancer patients and found a positive correlation between $f \times D^*$ and K^{trans} . Interestingly, they report an f -value about half the value of our estimations ($17.02 \pm$

TABLE 5. Correlations between DSC- and DCE-MRI

	K^{trans}	k_{ep}	v_p	v_e
BF	0.29 (0.004)	0.05 (0.67)	0.44 (<0.001)	0.10 (0.35)
AUC_{30}	0.14 (0.17)	-0.23 (0.03)	0.08 (0.44)	0.34 (0.001)
AUC_{60}	0.15 (0.14)	-0.45 (<0.001)	0.08 (0.47)	0.45 (<0.001)

Spearman's Rank Correlation Coefficients r_s (P-values in parenthesis)

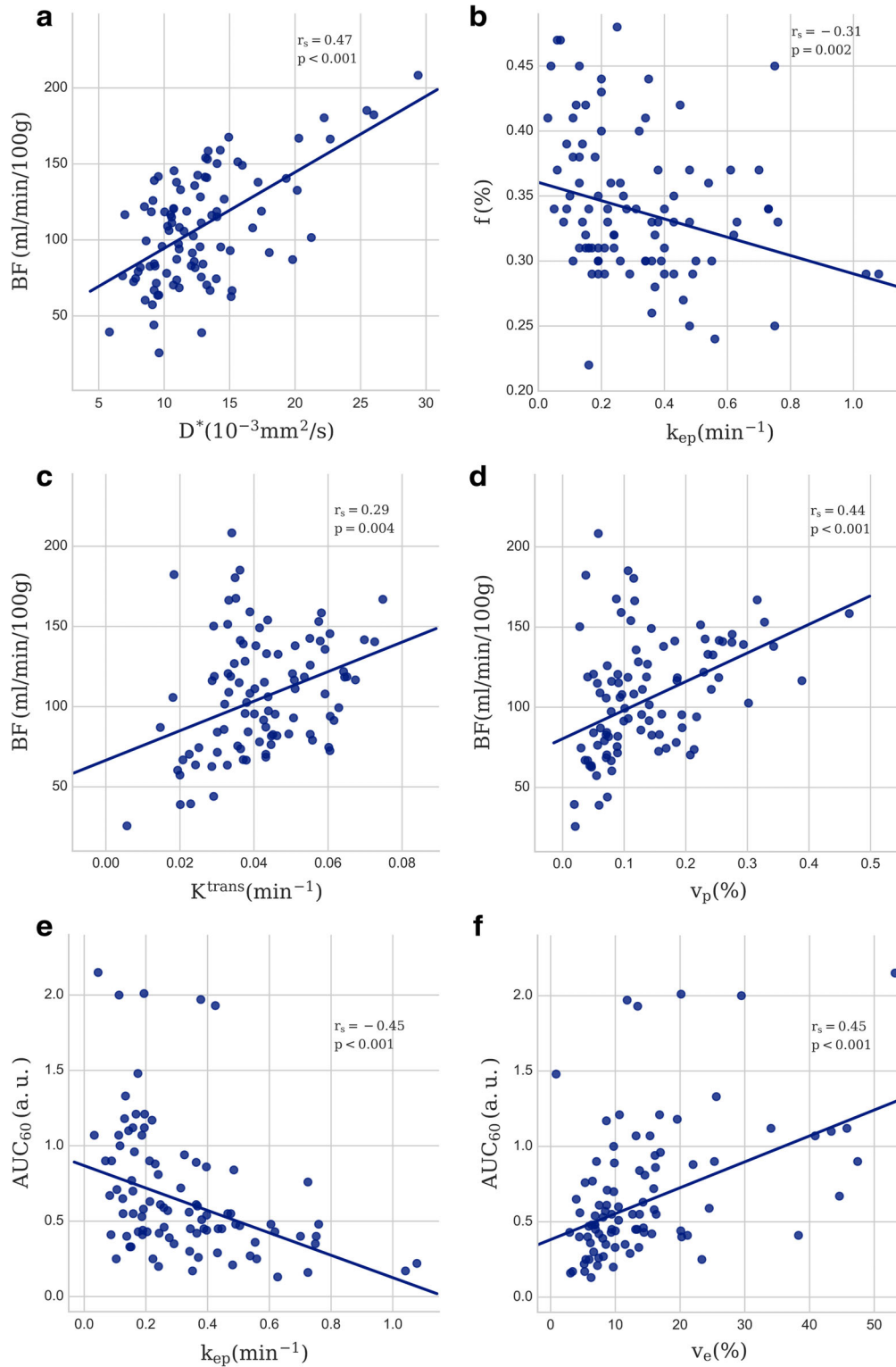


FIGURE 2: Scatterplot with the least square regression line of the most prominent results, (a) BF vs. D^* , (b) f vs. k_{ep} , (c) BF vs. K^{trans} , (d) BF vs. v_p , (e) AUC_{60} vs. k_{ep} , (f) AUC_{60} vs. v_e . Spearman's rank correlation coefficients (r_s) and P-values are indicated.

8.37% vs. $33 \pm 3.4\%$). Given that their investigations are with a superior diffusion sequence (3.0T and 16 b-values), one would assume their estimate to be more accurate. However, Xu et al,²⁹ who also did IVIM-analysis on 3.0T with 16 b-values, reports an f -value similar to ours ($>30\%$), and it is therefore not likely that the diffusion sequence we used is

the source of disagreement. Parameters from the IVIM analysis should, at least in theory, be more comparable between centers than for instance parameters from DCE- and DSC-MRI, and the repeatability and conformance of these parameters are of great interest and importance when comparing studies. It is therefore interesting, but not easily addressed,

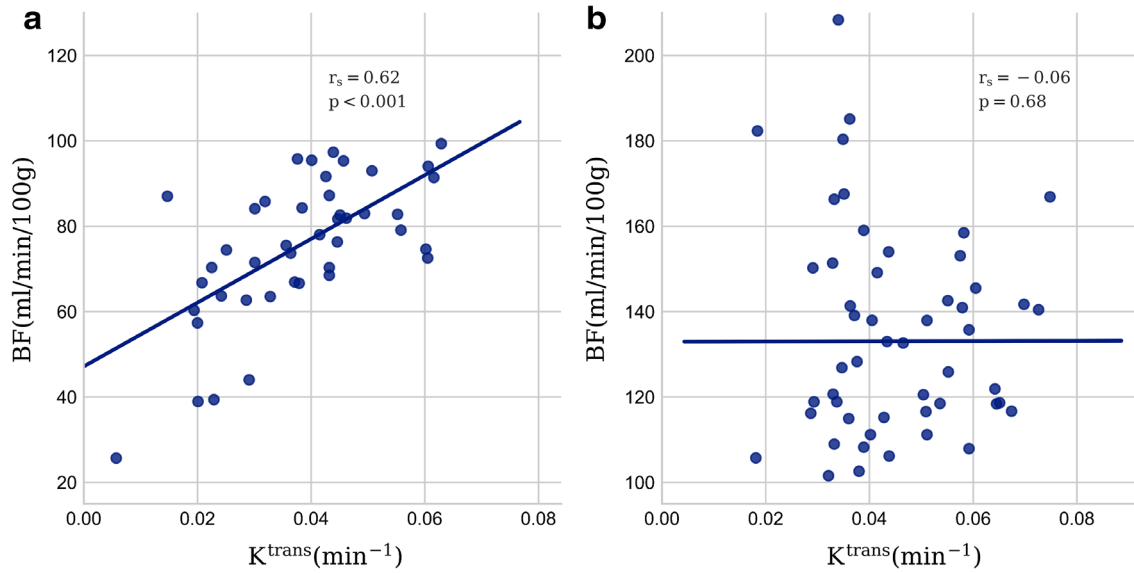


FIGURE 3: Scatterplot showing the correlation between BF and K^{trans} separated in populations with (a) low (<100) and (b) high (>100 ml/min/100 g) BF . Spearman's rank correlation coefficients (r_s) and P -values are indicated.

whether these differences could be attributed to the imaging performance or the algorithms used for analyzing the data.

We used the same AIF for analysis of the DSC and the DCE data, without adjusting for the different AIF amplitude of the R_2^* -response compared with the R_1 -response, as this will only have a linear and constant scaling effect on all parameters. Since the study was focused on parameter correlations between the different methods and not on absolute quantification, this scaling effect should not influence the results.

In a recent article,³⁰ Le Bihan mentions a common concern with the IVIM approach; the attenuation of the signal as it approaches higher b -values results in the signal reaching the "noise floor," where the signal is completely masked by the

noise. We therefore checked our results by doing the curve fitting to the biexponential curve both with and without the highest $b = 1300$ s/mm² value, which only resulted in linear shifts in the absolute value for all parameters and suggested that the curve fitting was adequately robust.

Our results would have been strengthened by the inclusion of a gold standard for perfusion measurements. There is, however, at present no clear gold standard for this purpose outside the CNS, and for this reason both DCE-, DSC-, and IVIM-MRI are proposed as methods for obtaining hemodynamic parameters that reflect perfusion. All these methods have limitations. Perfusion and volume estimates by DSC-MRI may be particularly challenging outside the CNS due to both kinetic model limitations (CA extravasation), uncertainty in AIF detection, and technical challenges relating to susceptibility artifacts and motion. Dynamic MRI acquisitions are particularly challenging in the pelvic cavity region due to susceptibility artifacts from gas-pockets and bowel motion; in addition, large susceptibility effects can occur when the contrast agent accumulates in the bladder. Bowel motion and susceptibility artifacts from gas-pockets are also a concern with DWI for the IVIM approach. Motion and susceptibility artifacts made it difficult to coregister smaller tumor volumes than 5 cm³, and they were excluded. We also experienced timing issues with the contrast administration after a software update, since this multiecho sequence was taken as part of a split dynamics sequence, interleaved with high spatial resolution images.³¹ However, by focusing on comparing these models against each other and finding a moderate correlation regardless of the limitations and uncertainties in these estimations, the hypothesis that both these methods can be used for perfusion imaging in rectal tumors is strengthened. We have further shown that by acquiring multiecho contrast-based MRI data, two separate dynamic series can be generated reflecting

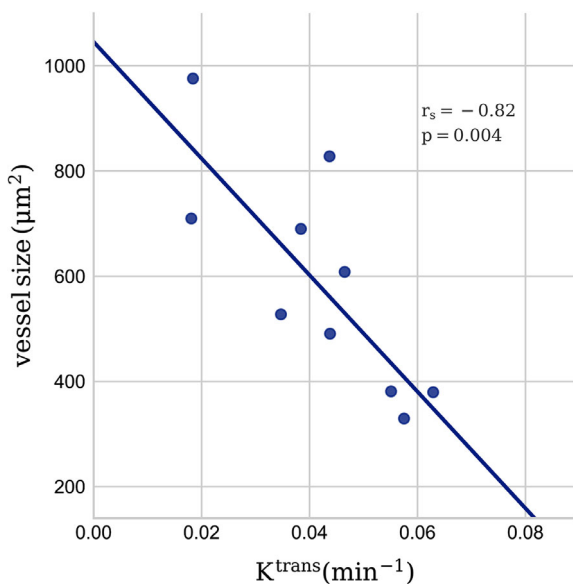


FIGURE 4: Scatterplot showing the correlation between vessel size quantified from CD34-based immunohistochemistry of excised tumors and K^{trans} from DCE-MRI. Spearman's rank correlation coefficient (r_s) and P -values are indicated.

different contrast mechanisms and possibly different underlying hemodynamic tissue properties.

As this was a single-center study, no comparison of parameters between imaging modalities from different vendors or with different field strength could be done. The patient population was heterogeneous, comprised of patients from many stages of rectal cancer, and so the underlying biology of the tumors may differ, and the biological interpretation of the measured parameters may vary within the patient population. However, this heterogeneity also ensures that the patient population is representative of the average rectal cancer patient in the clinic.

In conclusion, in rectal tumors, we observed a linear correlation between D^* from IVIM imaging and BF obtained from the R_2^* -curve. In addition, we found several other correlations between parameters derived from DSC-MRI, DCE-MRI, and IVIM. However, the interpretation of these parameters may depend on the underlying biology, the choice of kinetic models, and the MRI acquisition protocols used. The observed negative correlation between the contrast agent transfer constant, K^{trans} , from DCE-MRI and mean vessel size from IHC supports a dependence of K^{trans} on mean tumor vessel surface area.

Acknowledgments

Contract grant sponsor: South-Eastern Norway Regional Health Authority; Contract grant numbers: 2014012, 2015048, 2016050; Contract grant sponsor: Akershus University Hospital; Contract grant numbers: 267940, 268938; Contract grant sponsor: Olav Raagholt and Gerd Meidel Raagholt Research Foundation.

References

- Tong T, Sun Y, Gollub MJ, et al. Dynamic contrast-enhanced MRI: Use in predicting pathological complete response to neoadjuvant chemoradiation in locally advanced rectal cancer. *J Magn Reson Imaging* 2015;42:673–680.
- Shen FU, Lu J, Chen L, Wang Z, Chen Y. Diagnostic value of dynamic contrast-enhanced magnetic resonance imaging in rectal cancer and its correlation with tumor differentiation. *Mol Clin Oncol* 2016;4:500–506.
- Kanda T, Ishii K, Kawaguchi H, Kitajima K, Takenaka D. High signal intensity in the dentate nucleus and globus pallidus on unenhanced T1-weighted MR images: Relationship with increasing cumulative dose of a gadolinium-based contrast material. *Radiology*. 2014;270:834–841.
- Errante Y, Cirimele V, Mallio CA, Di Lazzaro V, Zobel BB, Quattrocchi CC. Progressive Increase of T1 Signal Intensity of the Dentate Nucleus on Unenhanced Magnetic Resonance Images Is Associated With Cumulative Doses of Intravenously Administered Gadodiamide in Patients With Normal Renal Function, Suggesting Dechelation. *Invest Radiol*. 2014;49:685–690.
- Bihan DL, Breton E, Lallemand D, Aubin ML, Vignaud J, Laval-Jeantet M. Separation of diffusion and perfusion in intravoxel incoherent motion MR imaging. *Radiology* 1988;168:497–505.
- Sun H, Xu Y, Song A, Shi K, Wang W. Intravoxel incoherent motion MRI of rectal cancer: Correlation of diffusion and perfusion characteristics with prognostic tumor markers. *AJR Am J Roentgenol* 2018;210:W139–w147.
- Federau C. Intravoxel incoherent motion MRI as a means to measure in vivo perfusion: A review of the evidence. *NMR Biomed* 2017;30:e3780.
- Østergaard L. Principles of cerebral perfusion imaging by bolus tracking. *J Magn Reson Imaging* 2005;22:710–717.
- Grøvik E, Redalen KR, Storås TH, et al. Dynamic multi-echo DCE- and DSC-MRI in rectal cancer: Low primary tumor K_{trans} and peak are significantly associated with lymph node metastasis. *J Magn Reson Imaging* 2017;46:194–206.
- Bisdas S, Braun C, Skardelly M, et al. Correlative assessment of tumor microcirculation using contrast-enhanced perfusion MRI and intravoxel incoherent motion diffusion-weighted MRI: Is there a link between them? *NMR Biomed* 2014;27:1184–1191.
- Marzi S, Stefanetti L, Sperati F, Anelli V. Relationship between diffusion parameters derived from intravoxel incoherent motion MRI and perfusion measured by dynamic contrast-enhanced MRI of soft tissue tumors. *NMR Biomed* 2016;29:6–14.
- Patel J, Sigmund EE, Rusinek H, Oei M, Babb JS, Taouli B. Diagnosis of cirrhosis with intravoxel incoherent motion diffusion MRI and dynamic contrast-enhanced MRI alone and in combination: Preliminary experience. *J Magn Reson Imaging* 2010;31:589–600.
- Lambregts DMJ, Maas M, Stokkel MPM, Beets-Tan RGH. Magnetic resonance imaging and other imaging modalities in diagnostic and tumor response evaluation. *Semin Radiat Oncol* 2016;26:193–198.
- Østergaard L, Weisskoff RM, Chesler DA, Gyldensted C, Rosen BR. High resolution measurement of cerebral blood flow using intravascular tracer bolus passages. Part I: Mathematical approach and statistical analysis. *Magn Reson Med* 1996;36:715–725.
- Rempp KA, Brix G, Wenz F, Becker CR, Gückel F, Lorenz WJ. Quantification of regional cerebral blood flow and volume with dynamic susceptibility contrast-enhanced MR imaging. *Radiology* 1994;193:637–641.
- Bjørnerud A, Emblem KE. A fully automated method for quantitative cerebral hemodynamic analysis using DSC-MRI. *J Cereb Blood Flow Metab* 2010;30:1066–1078.
- Wu O, Østergaard L, Weisskoff RM, Benner T, Rosen BR, Sorensen AG. Tracer arrival timing-insensitive technique for estimating flow in MR perfusion-weighted imaging using singular value decomposition with a block-circulant deconvolution matrix. *Magn Reson Med* 2003;50:164–174.
- Tofts PS. Modeling tracer kinetics in dynamic Gd-DTPA MR imaging. *J Magn Reson Imaging* 1997;7:91–101.
- Mikalsen LT, Dhakal HP, Bruland OS, Nesland JM, Olsen DR. Quantification of angiogenesis in breast cancer by automated vessel identification in CD34 immunohistochemical sections. *Anticancer Res* 2011;31:4053–4060.
- Sourbron SP, Buckley DL. On the scope and interpretation of the Tofts models for DCE-MRI. *Magn Reson Med* 2011;66:735–745.
- Henkelman RM. Does IVIM measure classical perfusion? *Magn Reson Med* 1990;16:470–475.
- Sun H, Xu Y, Xu Q, et al. Correlation between intravoxel incoherent motion and dynamic contrast-enhanced magnetic resonance imaging parameters in rectal cancer. *Acad Radiol* 2018; doi: <https://doi.org/10.1016/j.acra.2018.08.012> [Epub ahead of print].
- Kim YE, Lim JS, Choi J, et al. Perfusion parameters of dynamic contrast-enhanced magnetic resonance imaging in patients with rectal cancer: Correlation with microvascular density and vascular endothelial growth factor expression. *Korean J Radiol* 2013;14:878–885.
- Liu C, Wang K, Chan Q, et al. Intravoxel incoherent motion MR imaging for breast lesions: Comparison and correlation with pharmacokinetic evaluation from dynamic contrast-enhanced MR imaging. *Eur Radiol* 2016;26:3888–3898.
- Fujima N, Yoshida D, Sakashita T, et al. Intravoxel incoherent motion diffusion-weighted imaging in head and neck squamous cell carcinoma: Assessment of perfusion-related parameters compared to

- dynamic contrast-enhanced MRI. *Magn Reson Imaging* 2014;32:1206–1213.
26. Bihan DL, Turner R. The capillary network: A link between ivim and classical perfusion. *Magn Reson Med* 1992;27:171–178.
 27. Bjørnerud A, Sorensen AG, Mouridsen K, Emblem KE. T1- and T2*-dominant extravasation correction in DSC-MRI: Part I—Theoretical considerations and implications for assessment of tumor hemodynamic properties. *J Cereb Blood Flow Metab* 2011;31:2041–2053.
 28. Leu K, Boxerman JL, Cloughesy TF, et al. Improved leakage correction for single-echo dynamic susceptibility contrast perfusion MRI estimates of relative cerebral blood volume in high-grade gliomas by accounting for bidirectional contrast agent exchange. *Am J Neuroradiol* 2016;37:1440–1446.
 29. Xu Q, Xu Y, Sun H, et al. Quantitative intravoxel incoherent motion parameters derived from whole-tumor volume for assessing pathological complete response to neoadjuvant chemotherapy in locally advanced rectal cancer. *J Magn Reson Imaging* 2018;48:248–258.
 30. Le Bihan D. What can we see with IVIM MRI? *NeuroImage* 2017;187:56–67.
 31. Grøvik E, Bjørnerud A, Storås TH, Gjesdal K-I. Split dynamic MRI: Single bolus high spatial-temporal resolution and multi contrast evaluation of breast lesions. *J Magn Reson Imaging* 2014;39:673–682.